Anharmonic phonons in few-layer MoS_2: Raman spectroscopy of ultralow energy compression and shear modes

Mohamed Boukhicha,[1] Matteo Calandra,[1,*] Marie-Aude Measson,[2] Ophelie Lancry,[3] and Abhay Shukla[1,†]

[1]*Université Pierre et Marie Curie, IMPMC, CNRS UMR7590, 4 Place Jussieu, 75005 Paris, France*

[2]*Laboratoire Matériaux et Phénomènes Quantiques UMR 7162 CNRS, Université Paris Diderot-Paris 7, 75205 Paris cedex 13, France*

[3]*HORIBA Jobin Yvon S.A.S., 231 rue de Lille, 59650 Villeneuve d'Ascq, France*

(Received 16 January 2013; revised manuscript received 15 April 2013; published 28 May 2013)

Molybdenum disulfide (MoS_2) is a promising material for making two-dimensional crystals and flexible electronic and optoelectronic devices at the nanoscale. MoS_2 flakes can show high mobilities and have even been integrated in nanocircuits. A fundamental requirement for such use is efficient thermal transport. Electronic transport generates heat which needs to be evacuated, more crucially so in nanostructures. Anharmonic phonon-phonon scattering is the dominant intrinsic limitation to thermal transport in insulators. Here, using appropriate samples, ultralow energy Raman spectroscopy and first-principles calculations, we provide a full experimental and theoretical description of compression and shear modes of few-layer (FL) MoS_2. We demonstrate that the compression modes are strongly anharmonic with a marked enhancement of phonon-phonon scattering as the number of layers is reduced, most likely a general feature of nanolayered materials with weak interlayer coupling.

DOI: 10.1103/PhysRevB.87.195316 PACS number(s): 63.20.dk, 63.20.Ry, 63.22.−m

I. INTRODUCTION

Bulk MoS_2 is made of vertically stacked layers (single formula unit consisting of a Mo sheet sandwiched between two S sheets) weakly held together by van der Waals forces, with two layers per unit cell. While MoS_2 is an indirect gap semiconductor, it displays a crossover to a direct gap semiconductor with a resulting marked increase of photoluminescence upon reduction of crystal thickness down to one layer.[1]

In the case of a layered hexagonal system, the shearing modes are twofold degenerate as there are two equivalent in-plane shear directions. Generally an N-layer flake has $2*(N-1)$ shearing modes and $N-1$ compression-extension (noted compression henceforth) modes. Thus, while single layer MoS_2 should have neither one nor the other mode, in FL MoS_2 additional modes should appear with respect to bulk or the bilayer which both have two degenerate shear modes and one compression mode.

Both modes, importantly, are expected at very low energies since the interlayer interaction in MoS_2 is weak ($\omega_\nu < 55\ \mathrm{cm}^{-1}$ or 74 K). Therein lies their relevance to transport, both thermal and electronic.[2–7] At room temperature these phonon modes are all thermally populated and influence thermal transport via phonon scattering with defects and impurities or via phonon-phonon scattering. As anharmonicity is an intrinsic mechanism, in clean samples it is the dominant limitation to the thermal conductivity. Determining the behavior of these modes as a function of the flake thickness is of the greatest importance for nanoelectronic devices based on MoS_2.

Recently low-energy Raman modes in graphene[8] and MoS_2[9–11] were measured for FL flakes on p-doped Si substrates. In Ref. 9 only a single shear mode was detected and no compression modes were seen. Low-energy modes are weak in intensity and, to eliminate a broad low-energy background due to inelastic scattering of free carriers in the p-doped substrate,[12] these spectra were recorded in crossed geometry (i.e., the polarization of the outcoming light is perpendicular to that of the incident beam) where all compression modes are forbidden. In Ref. 11, beside the shearing mode detected in Ref. 9, a second feature was detected. No polarization analysis of the Raman spectra was performed and one of the features was attributed to a compression mode from a fit to a $1/N$ behavior (N = number of layers). In Ref. 10 a detailed study of shearing and compression modes up to 19 layers has been carried out. The authors were able to classify the low-energy Raman peaks in two groups, namely those that stiffen with increasing N and those that soften with increasing N. Then using a chain model they were able to build fan diagrams and obtain MoS_2 shearing and compression strength. No first-principles calculations of the Raman spectra were carried out.

In this work we measure low-energy Raman spectra as a function of the number of layers in multilayer MoS_2. We overcome the difficulty related to the presence of a broad low-energy background due to inelastic scattering of free carriers in the p-doped substrate[12] by using FL MoS_2 on borosilicate glass substrates. We measure shear and compression modes from one to five layers. By performing first-principles calculations of the position[13] and intensity[14] of Raman peaks we obtain a complete understanding of shear and compression modes in FL MoS_2. We also analyze theoretically the dependence of the main shearing mode as a function of applied pressure and show that it behaves linearly at low pressure (below 1 GPa).

II. EXPERIMENT

The samples are made using the anodic bonding method which bonds a bulk flake to a borosilicate glass substrate[15,16] at a temperature between 130 and 200 °C and a high voltage which may range from 200 to 1500 V. The flake is then mechanically cleaved leaving large few-layer samples on the glass (see Fig. 1). The sample used in this work is exceptional in that it provides all different thicknesses used on the same flake, making comparison easy. The sample thickness was

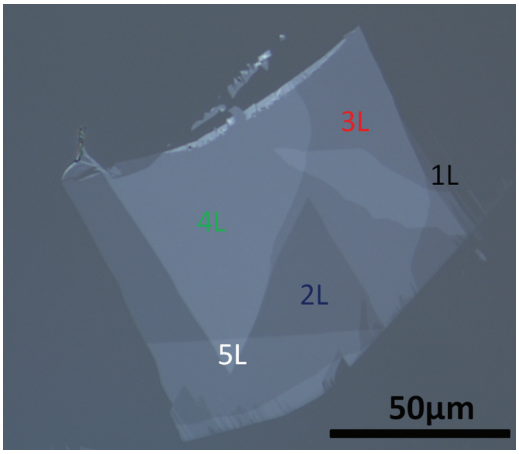

FIG. 1. (Color online) The few-layers MoS_2 flake made by anodic bonding and used for the experiment. The number of layers is indicated.

identified first by optical contrast and then confirmed by atomic force microscope and Raman spectroscopy,[17] as shown in Fig. 2.

Micro-Raman spectra of the FL MoS_2 are measured (532 nm radiation, ≈1 mW laser power) in backscattering configuration with parallel and crossed polarization geometry. To enable measurements down to ≈10 cm^{-1} on a single-grating spectrometer (LabRAM HR from HORIBA Jobin Yvon), an ultralow wave number filtering (ULF™) accessory for 532 nm wavelength was used. These volume Bragg gratings can be fabricated with diffraction efficiencies as high as 99.99% and the linewidth narrower than 1 cm^{-1} at FWHM that corresponds to 3–4 cm^{-1} cut-off frequency at −60 dB from maximum. They also make a unique notch filter for Rayleigh light rejection by sequential cascading of several Bragg notch filters, enabling ultralow frequency Raman measurements with single stage spectrometers.[18,19] To avoid laser heating, a laser power of 1 mW was focused through a 50× or 100× microscope objectives.

In order to evaluate the actual temperature on the sample and to exclude laser heating, we measure for all thicknesses both Stokes and anti-Stokes features at high and low energy. We then determine the temperature as

$$T = \frac{\hbar\omega}{k_B} \ln\left\{\frac{I_S}{I_{AS}}\left(\frac{\omega_L+\omega}{\omega_L-\omega}\right)^4\right\}, \quad (1)$$

where ω is the Raman shift and ω_L is the pulsation of the laser light. For a more precise determination of the temperature we use the intensity of the high-energy A_{1g} and E_{2g} modes. We obtain $T \approx 360$ K. Thus the laser heating is ≈60 K, i.e., negligible.

III. THEORY

Calculations were performed by using density functional theory in the local density approximation.[20] The QUANTUM-ESPRESSO[13] package was used with norm-conserving pseudopotentials and a plane-wave cutoff energy of 90 Ry. Semicore states were included in Mo pseudopotential. All calculations were performed at 0 and 6 kbars uniaxial pressure, corresponding to the uniaxial pressure imposed in the anodic bonding procedure. The crystal structure at a given pressure is obtained by keeping the same in-plane experimental lattice parameter as in bulk samples. The interlayer distance is obtained by imposing a 6 kbars pressure with respect to the bulk experimental structure at 0 kbar. The distance between the plane is then kept constant for all N-layers flakes, but sulfur height, the only free parameter, is optimized following internal forces. Phonon frequencies, born-effective charges, and Raman tensor were calculated using a $8 \times 8 \times 1$ k-point grid for the monolayer and a $8 \times 8 \times 8$ for the bulk. Using this grid, phonon frequencies of shearing and compressing modes are converged with an accuracy of 1 cm^{-1}. Raman intensities were calculated with the method of Ref. 14 in the Placzek approximation.

The intensity of a mode ν is written as

$$I^{\nu} \propto I_0^{\nu}(n_{\nu}+1)/\omega_{\nu},$$

where ω_{ν} and n_{ν} are the phonon frequency and the occupation of the phonon mode ν. Moreover, $I_0^{\nu} = |\mathbf{e}_i \cdot \mathbf{A}\mathbf{e}_o|^2$, where $\mathbf{A}$ is the Raman tensor while $\mathbf{e}_i$ and $\mathbf{e}_o$ are the the polarization of the incident and scattered radiation, respectively. In Table I we give the calculated value of I_0^{ν} as a function of the layer

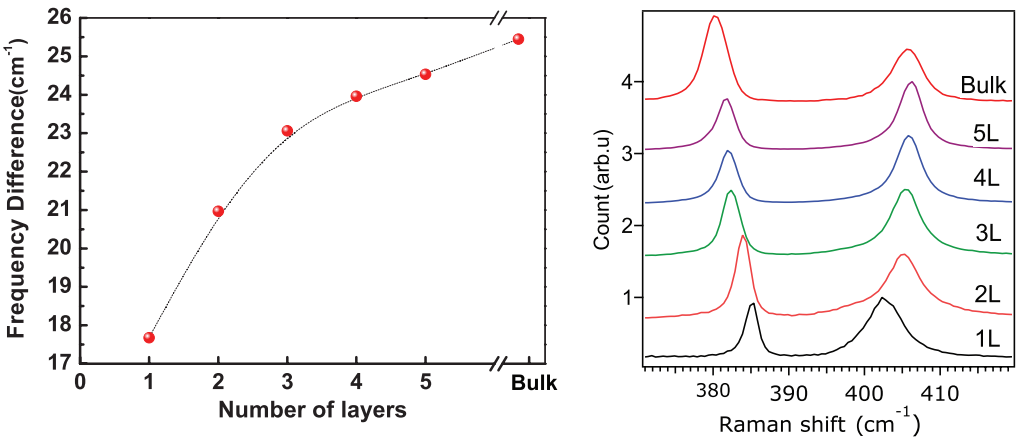

FIG. 2. (Color online) Energy difference of the E_{2g} and the A_{1g} phonon modes at high energy versus the number of layers (left) and experimental high-energy Raman spectra as a function of the layer number (right).

TABLE I. Raman intensity I_0^ν for different modes ν and as a function of the number of layers N for backscattering geometry (labeled ∥ geom.) and cross backscattering geometry. The intensity is normalized to the most intense low-energy mode (below 100 cm^{-1}). Note that in the two and three layer case, the compression mode has stronger intensity I_0^ν then the main shear mode, however the larger linewidth suppresses its I^ν.

ω_ν (cm^{-1})	$\mathbf{e}_i \parallel \mathbf{e}_o$	$\mathbf{e}_i \perp \mathbf{e}_o$
$N = 2$		
23.1	0.282	1.0
37.6	1.0	<0.001
$N = 3$		
16.31	<0.001	<0.001
26.43	1.0	<0.001
28.42	0.73	1.0
45.95	<0.001	<0.001
$N = 4$		
12.56	<0.005	<0.001
20.53	0.69	< 0.001
23.34	<0.001	
30.57	1.0	1.0
47.45	<0.001	<0.001
48.90	<0.001	0.13
$N = 5$		
10.04	<0.001	<0.001 0
16.61	0.42	<0.001
19.18	0.02	< 0.002
26.50	<0.001	<0.001
31.21	1.0	1.0
31.25	< 0.001	<0.001
42.62	0.17	<0.001
50.45	<0.001	<0.001

number and the experimental geometries for the low-energy modes.

The experimental spectrum is then obtained as

$$I(\omega) \propto \sum_\nu I^\nu \delta(\omega - \omega_\nu). \quad (2)$$

In order to compare with experiments, the Dirac δ functions are convoluted with the experimental linewidths.

At ambient pressure, the calculated frequencies are in excellent agreement with previous calculations,[21] however they disagree with the calculations of Ref. 11. In particular, for a MoS_2 bilayer at zero uniaxial pressure and using the experimental in-plane lattice parameter we find 20 cm^{-1} for the main shearing mode. Performing structural optimization of both in-plane and interlayer distance (always keeping the same empty region between periodic images) we find 24.49 cm^{-1} for the shear mode. Thus the shear phonon frequency weakly depends on the choice of the experimental or theoretical in-plane lattice parameters in the calculation. This has to be compared with 22 cm^{-1} in our experimental Raman data, with ≈23 cm^{-1} in experimental Raman data of Ref. 11, and with ≈19.5 cm^{-1} in Raman data of Ref. 9. In Ref. 11 the shearing mode was calculated at 35.3 cm^{-1} using the theoretical lattice structure and the LDA approximation which would correspond to a very large applied pressure, not relevant to the experiments in consideration.

IV. GENERAL DISCUSSION ON SECONDARY SHEAR AND COMPRESSION MODES

As already stressed in the Introduction, a MoS_2 N-layer flake has $2 * (N - 1)$ twofold degenerate shearing modes and $N - 1$ compression modes. Shear modes correspond to rigid layer displacements perpendicular to the c axis. The twofold degeneracy depends on the crystal symmetry of the lattice. In MoS_2, for example, it is equivalent to rigidly shift a subset of layers with respect to one in-plane crystalline axis or the other. For an N-layer flake (with $N < 5$) the rigid layer displacement patterns are schematically illustrated in Fig. 3 (right). The hardest shear mode always corresponds to the rigid shift of the innermost layers, these being more tightly bound by the bilateral interaction with the other layers. The hardest (also named principal or primary) shear mode is labeled S_n, where n is the number of layers. The shear mode S_n is Raman active and is also the most intense of all the shear modes. As the number of layer increases, there are more possibilities of rigidly shifting layers. For example, in a three layer flake it is possible to shift only the top (or bottom) layer keeping the other two fixed. This mode is however softer then the main shear mode, as the outer layers have only one nearest neighbor layer with weaker binding. In our case and at 6 kbars uniaxial pressure, the secondary shear mode is calculated to be at 16.3 cm^{-1}, but with essentially zero Raman intensity (although this mode is not forbidden by symmetry). In the general case of an N-layer flake, there are $(N - 1)$ independent ways of shifting a subset of layers with respect to the others and their energies lie between that of the (softest) secondary shear mode related to the shift of extremal layer and the (hardest) main shear mode.

Compression (or extension) modes are rigid vibrations of the layers in the direction perpendicular to the layers. For an N-layer flake (with $N < 5$) the rigid layer displacement pattern are schematically illustrated in Fig. 3 (left). As in the

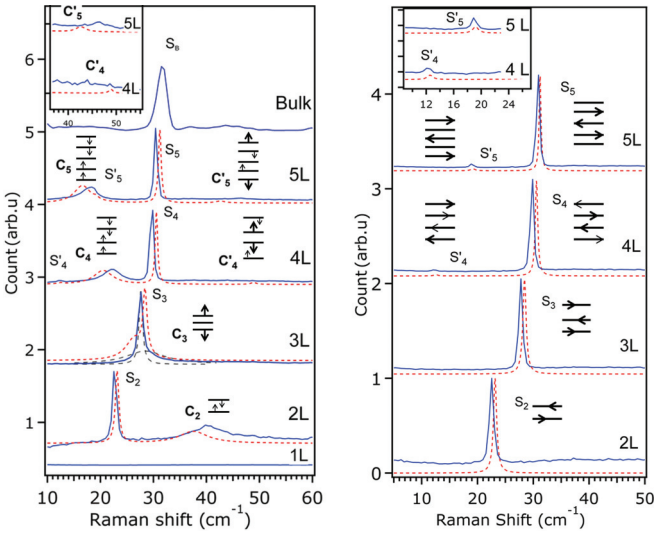

FIG. 3. (Color online) Experimental (blue) and theoretical (red dashed) Raman spectra in parallel (left) and crossed (right) configuration. The inset shows a blow up of the low-energy region. Also shown are the schematized MoS_2 layer movements for the compression (left) and the shear (right) modes. All arrows may be simultaneously reversed and the size corresponds to the amplitude.

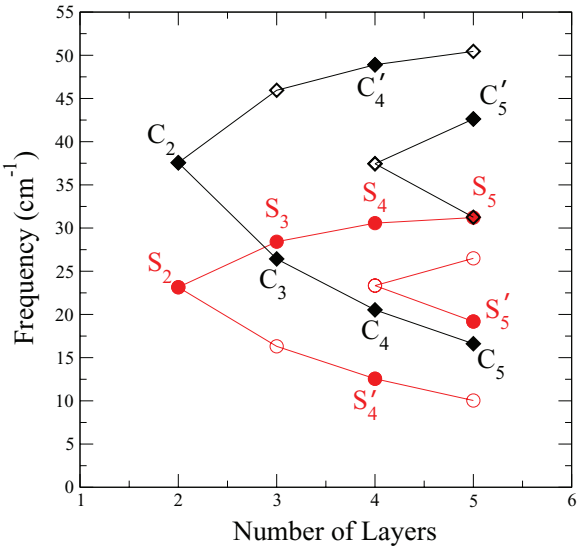

FIG. 4. (Color online) Fan diagram of calculated shear (red) and compression (black) mode frequencies as a function of the number of layers. Full symbols represent modes visible in our Raman experiments in parallel and crossed configuration. The labels of the different modes are the same as in Fig. 3.

case of shear modes it is possible to identify a primary or main compression mode. The main compression mode is the one corresponding to (i) the lower half of the layers shifting in the same direction and (ii) the higher half of the layers in the opposite direction. The main compression mode (labeled C_n) is the softest compression mode. Secondary compression modes arise when the top half (respectively, bottom half) layers are not all displaced in the same direction. Secondary compression modes are higher in energy than the main compression mode (see Fig. 4, the rigid layer model of 23, and the discussion below).

V. RESULTS

In Fig. 3 we show measured and calculated spectra in parallel and crossed geometries. The peaks are normalized to the main shear mode intensity and the theoretical spectra are convoluted by the experimental linewidth.

By comparing the main shear mode (labeled S_n) to existing measurements,[9] we notice that in our samples this mode is systematically harder by $\approx$3 cm^{-1}. We attribute this to the anodic bonding method which binds flakes to a glass substrate electrostatically due to the creation of a space charge in the substrate. This also generates an electrostatic pressure on the flake bound to the substrate. Knowing the depth of this space charge layer (1–2 μm) this uniaxial pressure along the c axis[22] can be estimated to be in the range of 3–6 kbars.

We thus performed first-principles calculations as a function of pressure and obtain an essentially linear behavior of the main shearing mode for a MoS_2 bilayer as a function of uniaxial pressure, with a linear coefficient that is 1.17 cm^{-1}/kbar (the second order coefficient in the fit is 0.04 cm^{-1}/kbar^2). Comparing the measured spectra with the calculated ones for 6 kbars uniaxial pressure, we find remarkable agreement.

Besides the main shear mode, already detected in Refs. 9 and 11, we measure secondary shear (S_n and S'_n) and compression (labeled C_n and C'_n) modes (see Figs. 4 and 3). In Ref. 11 only the C_n compression mode was detected.

The compression mode is clearly visible in two, four, and five layer samples and less so in the three layer sample because it coincides in energy with the shear mode. In the four and five layer samples, theory also accounts for the additional shear (S'_n) and compression (C'_n) modes detected in experiments.

It is worthwhile to recall that the energy of shear and compression modes can either increase or decrease as a function of the number of layers N, as shown in the fan diagrams in Ref. 23 and in Fig. 4. In FL MoS_2, the energy of Raman visible E_g shear modes increases with the number of layers, while that of Raman visible A_{1g} compression modes decreases.

The qualitative behavior of the position of the main shear and compression modes as a function of layer number can be easily understood in a simple rigid-layer (or chain) model.[24] We write for the S_n shear-mode frequency

$$\omega_S = \frac{1}{\sqrt{2}\pi c}\sqrt{\frac{\alpha_S}{\mu}}\sqrt{1+\cos\left(\frac{\pi}{N}\right)}, \tag{3}$$

where $\mu = 30.75\,\mathrm{kg/m^2}$ is the rigid layer mass per unit and α_S is the shearing strength. The C_n compression mode behaves as

$$\omega_C = \frac{1}{\sqrt{2}\pi c}\sqrt{\frac{\alpha_C}{\mu}}\sqrt{1-\cos\left(\frac{\pi}{N}\right)} \tag{4}$$

and α_C is the compression strength. From the experimental curves we obtain $\alpha_S = 27.44\times10^{18}\,\mathrm{N/m^3}$, twice the value in graphene,[8,23] and $\alpha_C = 420.44\times10^{18}\,\mathrm{N/m^3}$. Both these effects are in part explained by the smaller interlayer distance in MoS_2 (the sulfur-sulfur distance along c is 3.03 Å) with respect to graphite (3.35 Å). The agreement between Eqs. (3) and (4) and experimental data is shown in Fig. 5, validating the chain model and the extracted values of α_S and α_C.

In Fig. 5 we also plot the variation of the linewidth γ for the S_n shear and the C_n compression modes as a function of the number of layers n. Shear mode linewidth is resolution limited, while all the compression modes are very broad (roughly 7 times broader), the linewidth of the C_2 mode being the largest. As the broadening is inversely proportional to the phonon-phonon scattering time, our result indicates that the phonon scattering time of compression modes is approximately 7 times smaller than that of shear modes. Thus the contribution of optical modes to the intrinsic thermal conductivity of MoS_2 flakes is dominated by scattering to compression modes. In a MoS_2 bilayer, the scattering time of compression modes is nearly 9 times smaller than that of shear modes.

The compression modes linewidths are generally larger than those of shearing modes as the potential is more anharmonic for a displacement perpendicular to the MoS_2 layers than for a shearing displacement. In the case of C_2, the linewidth is enhanced with respect to C_n with $n > 2$ due to the fact that more channels for anharmonic decay are available. Indeed for $n > 2$, the compression mode is lower in energy (or at the same energy for $n = 3$) than the shearing mode. As such it can only decay into two acoustic modes of opposite momentum. In

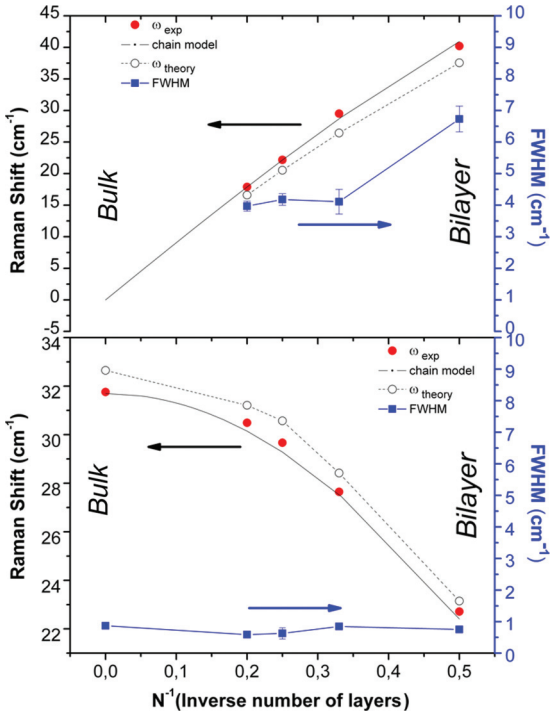

FIG. 5. (Color online) Energy and linewidth (γ) full-width half-maximum of compression (top) and shear (bottom) modes as a function of the inverse layer number.

the case $n = 2$, the compression mode is at roughly twice the energy of the shearing mode S_2. Thus the compression mode can decay into (i) two acoustic modes of opposite momentum, (ii) an acoustic and a shearing mode of opposite momentum, or (iii) two shearing modes of opposite momentum.

VI. CONCLUSION

In conclusion, we have measured primary and secondary shearing and compression modes in MoS_2 from one to five layers. The compression modes are found to be strongly anharmonic, with phonon-phonon scattering increasing upon reducing the number of layers. Thus compression modes represent the overriding optical phonon contribution to the intrinsic thermal conductivity of MoS_2 flakes, a crucial aspect of any use of these in future nano- or microelectronic devices. The relevance of our work is far reaching as compression modes are most likely strongly anharmonic in all flakes obtained from weakly interacting layered materials such as few-layer graphene, transition metal dichalcogenides, and topological insulators. In all these systems a crucial limit to thermal transport could be the anharmonicity of compression phonon modes.

ACKNOWLEDGMENTS

We acknowledge K. Gacem for help in sample preparation. This work was supported by French state funds managed by the ANR within the Investissements d'Avenir programme under reference ANR-11-IDEX-0004-02 and ANR-11-BS04-0019. Calculations were performed at the IDRIS supercomputing center.

*matteo.calandra@upmc.fr
†abhay.shukla@upmc.fr

[1] K. F. Mak, C. Lee, J. Hone, J. Shan, and T. F. Heinz, Phys. Rev. Lett. **105**, 136805 (2010).
[2] Q. H. Wang, K. Z. Kurosh, A. Kis, J. N. Coleman, and M. Strano, Nat. Nanotechnol. **7**, 699 (2012).
[3] B. Radisavljevic, A. Radenovic, J. Brivio, V. Giacometti, and A. Kis, Nat. Nanotechnol. **6**, 147 (2011).
[4] A. Castellanos-Gomez, M. Barkelid, A. M. Goossens, V. E. Calado, H. S. J. van der Zant, and G. A. Steele, Nano Lett. **12**, 3187 (2012).
[5] S. Kim, A. Konar, W. S. Hwang, J. H. Lee, J. Lee, J. Yang, C. Jung, H. Kim, J. B. Yoo, J. Y. Choi, Y. W. Jin, S. Y. Lee, D. Jena, W. Choi, and K. Kim, Nat. Commun. **3**, 1011 (2012).
[6] B. Radisavljevic, M. B. Whitwick, and A. Kis, ACS Nano **5**, 9934 (2012).
[7] H. Wang, L. Yu, Y.-H. Lee, Y. Shi, A. Hsu, M. L. Chin, L.-J. Li, M. Dubey, J. Kong, and T. Palacios, Nano Lett. **12**, 4674 (2012).
[8] P. H. Tan, W. P. Han, W. J. Zhao, Z. H. Wu, K. Chang, H. Wang, Y. F. Wang, N. Bonini, N. Marzari, N. Pugno, G. Savini, A. Lombardo, and A. C. Ferrari, Nat. Mater. **11**, 294 (2012).
[9] G. Plechinger, S. Heydrich, J. Eroms, D. Weiss, C. Schuller, and T. Korn, Appl. Phys. Lett. **101**, 101906 (2012).
[10] X. Zhang, W. P. Han, J. B. Wu, S. Milana, Y. Lu, Q. Q. Li, A. C. Ferrari, and P. H. Tan, Phys. Rev. B **87**, 115413 (2013).
[11] H. Zeng, B. Zhu, K. Liu, J. Fan, X. Cui, and Q. M. Zhang, Phys. Rev. B **86**, 241301(R) (2012).
[12] M. Chandrasekhar, U. Rössler, and M. Cardona, Phys. Rev. B **22**, 761 (1980).
[13] P. Giannozzi *et al.*, J. Phys.: Condens. Matter **21**, 395502 (2009).
[14] M. Lazzeri and F. Mauri, Phys. Rev. Lett. **90**, 036401 (2003).
[15] A. Shukla, R. Kumar, J. Mazher, and A. Balan, Solid State Commun. **149**, 718 (2009).
[16] K. Gacem, M. Boukhicha, Z. Chen, and A. Shukla, Nanotechnology **23**, 505709 (2012).
[17] C. Lee, H. Yan, L. E. Brus, T. F. Heinz, J. Hone, and S. Ryu, ACS Nano **4**, 2695 (2010).
[18] L. B. Glebov, in *Encyclopedia of SmartMaterials 2*, edited by M. Schwartz (John Wiley and Sons, New York, 2002), p. 770.
[19] A. L. Glebov *et al.*, Proc. SPIE **8428**, 84280C (2012).
[20] Appendix C of J. P. Perdew and A. Zunger, Phys. Rev. B **23**, 5048 (1981).
[21] A. Molina-Sanchez and L. Wirtz, Phys. Rev. B **84**, 155413 (2011).
[22] T. Anthony, Appl. Phys. Lett. **54**, 2419 (1983).
[23] K. H. Michel and B. Verberck, Phys. Rev. B **85**, 094303 (2012).
[24] N. W. Ashcroft and N. D. Mermin, *Solid State Physics* (Harcourt, New York, 1976), p. 433.